Received: 15 May 2023 | Revised: 22 June 2023 | Accepted: 11 July 2023

DOI: 10.1002/eom2.12399

RESEARCH ARTICLE

EcoMat FUNCTIONAL MATERIALS FOR GREEN ENERGY AND ENVIRONMENT WILEY

Aesthetic and efficient perovskite/Si tandem solar cells using luminescent down-shifting textured anti-reflection films

Eui Dae Jung | **Chan Ul Kim** | **Young Wook Noh** | **Seong Kuk Seo** | **Young Im Noh** | **Kyoung Jin Choi** | **Myoung Hoon Song**

Department of Materials Science and Engineering, Ulsan National Institute of Science and Technology (UNIST), Ulsan, Republic of Korea

Correspondence
Kyoung Jin Choi and Myoung Hoon Song, Department of Materials Science and Engineering, Ulsan National Institute of Science and Technology (UNIST), UNIST-Gil 50, Eonyang-eup, Ulju-gun, Ulsan 44919, Republic of Korea.
Email: choi@unist.ac.kr; mhsong@unist.ac.kr

Present addresses
Eui Dae Jung, Department of Electrical and Computer Engineering, University of Toronto, Toronto, Ontario, Canada; and Chan Ul Kim, Institute of Advanced Technology Development, Hyundai Motor Group, Seongnam, Republic of Korea.

Funding information
Korea Institute of Energy Technology Evaluation and Planning, Grant/Award Number: 20213091010010; National Research Foundation of Korea, Grant/Award Numbers: 2019M1A2A2072416, 2019K1A3A1A61091347, 2021M3H4A1A02051234

Abstract

Perovskite-based tandem cells are emerging as new photovoltaic (PV) cells with a high efficiency that exceeds the efficiency limit of single-junction cells. Building-integrated PVs that require high efficiency are attractive, but aesthetics play key roles in these urban applications. One of the most challenging problems with respect to aesthetic PV cells is the efficiency loss due to color tuning. Here, we demonstrate for the first time lossless full-color tunable PV cells based on the use of textured luminescent down-shifting (LDS) films with LDS dyes with ultraviolet-selective absorption. The LDS anti-reflection (AR) films improve the perovskite/Si tandem cell efficiency by reducing the loss of parasitic UV absorption of the layers above the perovskite film due to LDS effect and the loss due to cell reflection due to the textured surface. Therefore, color tuning with LDS AR films can be used to produce highly aesthetic and efficient PV cells for urban applications.

KEYWORDS

anti-reflection (AR), building-integrated photovoltaics (BIPV), color tuning, colored solar cells, luminescent down-shifting (LDS), perovskite solar cells, tandem solar cells

1 | INTRODUCTION

Photovoltaic (PV) technology is the key to achieve greenhouse gas emission-free energy production by 2050.[1] Recently, perovskite solar cells have emerged, which

Eui Dae Jung and Chan Ul Kim contributed equally to this work.

have a high efficiency and are based on a low-cost solution process.[2,3] Furthermore, due to the simple bandgap tuning of the perovskite absorber and simple fabrication of semi-transparent cells with top transparent electrodes, perovskite-based tandem cells are intensively studied aiming at the commercialization of cost-effective PV cells exceeding the power conversion efficiency (PCE) limit of single-junction cells.[4–7] Among the PV applications for perovskite-based tandem cells, building-integrated photovoltaics (BIPVs) and vehicle-integrated photovoltaics (VIPVs) are highly attractive because perovskite-based tandem cells are suitable for the generation of high power in a limited installation area.[8,9] In contrast to conventional PV cells, which are built on the ground away from the point of demand, BIPVs and VIPVs can save costs with respect to land, frames, and electricity storage/transportation. However, the aesthetic aspects are crucial to the acceptance of PVs in these applications. Therefore, the color tuning of PV cells from a simple dark color to a wide range of colors with a high PCE is a key issue in BIPV and VIPV applications. The color tuning of PV cells with structural color based on the fabrication of a nanograting,[10] photonic crystals,[11,12] and microcavities[13–19] has been widely studied. Among the methods that can be used to obtain structural color, the distributed Bragg reflector (DBR) consists of multi-stacked layers of alternating materials with different refractive indexes. It is noteworthy because selective narrow-bandwidth reflection can be achieved by precisely controlling the thickness and refractive index of the materials. Yoo et al.[19] reported vivid color tuning of perovskite solar cells with a relative PCE loss ranging from 6% to 10% via narrow-bandwidth reflection using the DBR. However, structural color that requires fine nano- or microstructures is based on a sophisticated design involving complex fabrication processes and this structural color is disadvantageous for the scale-up.[8] Another disadvantage of color tuning of PV cells with structural color is that it is based on the reflection of illuminated light, which inevitably leads to the loss of light absorption in PVs and thus to PCE loss.

On the other hand, luminescent down-shifting (LDS), the process of converting one photon of light with a shorter wavelength to one photon of light with a longer wavelength, has been studied aiming at increasing the light absorbance and PCE of PV cells.[20] The LDS films containing LDS dyes in transparent host polymers are coated on the front side of the PV cells and the dyes convert the light. To increase the PCE of the PV cells using LDS films on the front of the PV cells, high photoluminescent quantum yields (PLQYs) of luminescent dyes in the host polymers are required. In addition, selective UV light absorption and the emission of LDS dyes from the low external quantum efficiency (EQE) region of the PV to the high EQE region are required. Unfortunately, increasing the PCE of the PV cell with LDS is inherently limited because dyes emit light isotropically and almost half of the emitted light escapes from the PV cell. However, light escaping from the PV cell with LDS can reach the human eyes, which is the key to lossless color tuning of PV cells.

Schlisske et al.[21] pioneered the color tuning of perovskite solar cells with LDS dyes. Each red, green, and blue light-emitting organic dye (Lumogen F series Red 300, Yellow 083, Violet 570, respectively) dispersed in poly(methyl methacrylate) (PMMA) host polymer was inkjet-printed on single-junction perovskite solar cells, allowing great degree of freedom in terms of shape and color. Although the concentration of dyes and the number of layers had been optimized, high absorption and high PLQY of LDS films could not be simultaneously achieved. To simultaneously achieve a high absorption and high PLQY of LDS films, the film thickness must be much higher to facilitate sufficient absorption, while the concentrations of LDS dyes must be kept low to prevent the aggregation of dyes and PLQY decrease. Furthermore, the Red 300 dye absorbs light at a wavelength of ~550 nm, which is the high EQE region of perovskite solar cells, resulting in a significant drop of the PCE.

In terms of PCE of PV cells, Jiang et al.[22] successfully increased PCE of perovskite/Si tandem solar cells with LDS. The $(Ba,Sr)_2SiO_4:Eu^{2+}$ phosphor was incorporated in the textured polydimethylsiloxane (PDMS) anti-reflection (AR) film. This LDS film convert the UV light to green light and reduce the reflection at the surface. The EQE between 300 and 400 nm was increased with increasing the concentration of $(Ba,Sr)_2SiO_4:Eu^{2+}$ phosphor, and short-circuit current density (J_{SC}) of perovskite/Si tandem cell was increased by 0.3 mA/cm^2. However, increasing the concentration of $(Ba,Sr)_2SiO_4:Eu^{2+}$ phosphor to fully absorb the UV light resulted in the increase of reflectance due to backward scattering because silicate-based phosphors have high refractive index than PDMS and the size of silicate-based phosphors (>5 μm) are much larger than the wavelength of incident light.[23] In addition, this insufficient UV light absorption of LDS films with low concentration silicate-based phosphors acts as a limitation for color tuning of PV cells due to low intensity of emitted light from LDS dye under solar light.

Therefore, efficient light emission of each of the three primary colors (red, green, and blue) of well-dispersed LDS dye molecules with UV selective absorption in thick host polymers are highly desirable to achieve a breakthrough in lossless color tuning of PV cells with LDS. For red and green emissions with UV-selective absorption, inorganic LDS dyes based on luminescent metal complexes are promising, which have larger Stokes shifts than organic LDS dyes.

With respect to high-efficiency tandem cells for BIPV and VIPV applications, color tuning with LDS dyes is superior to color tuning with structural color. Current matching between the top and bottom cells is essential to achieve highly efficient tandem cells,[24] but color tuning with structural color causes the loss of light absorption (even color-dependent) in the top cell, resulting in the failure of current matching. In addition, surface texturing in tandem cells is effective at reducing the light reflection over a wide wavelength range,[25] but color tuning using structural color is not compatible with textured surfaces. On the other hand, current matching can be maintained by lossless color tuning with LDS dyes, which is compatible with surface texturing for high-efficiency tandem cells.

In this study, we selected the UV-absorbing LDS dyes (1,10-Phenanthroline)tris[4,4,4-trifluoro-1-(2-thienyl)-1,3-butanedionato]europium(III) ($Eu(TTA)_3Phen$) for red emission, Tris(2-phenylpyridinato)iridium(III) ($Ir(ppy)_3$) for green emission, and 4,4′-Bis(9-ethyl-3-carbazovinylene)-1;4,4′-Bis(9-ethyl-3-carbazovinylene)-1,1′-biphenyl (BCzVBi) for blue emission. Both high absorption and PLQY of LDS dyes in the films were successfully obtained, using well-dispersed dyes in thick (>200 μm) poly(ethylene-co-vinyl acetate) (EVA) host polymer films. UV-selective absorption, high PLQY, and high color purity of all red, green, and blue emissive LDS films were confirmed by optical analysis. In addition, a design with full color tunability and free shape was established via the simple intuitive mixing of red-, green-, and blue-emitting dyes and selective arrangement of dyes. Surface-textured LDS films were attached to perovskite/Si tandem cells for AR as well as color tuning. The PCE of perovskite/Si tandem cells with surface-textured film significantly increased from 20.24% to 22.62%, representing an 11.8% relative improvement after introduction of surface-textured film due to AR effect. Finally, lossless red (PCE of 22.89%, 13.1% relative increase), green (PCE of 22.51%, 11.2% relative increase), and blue (PCE of 23.00%, 13.6% relative increase) tandem cells were successfully achieved for the first time by introducing LDS dyes into textured AR films.

2 | RESULTS AND DISCUSSION

Figure 1A shows the chemical structures of EVA, $Eu(TTA)_3Phen$, $Ir(ppy)_3$, and BCzVBi. The EVA was chosen as the host polymer for the LDS AR film because of its high transparency (even in the UV range), ease of processing with organic solvents and heat, and high solubility of the dyes in EVA, which leads to good dispersion of the dyes in EVA film, without aggregation.[26–28] Red-, green-, and blue-emitting dyes, that is, $Eu(TTA)_3Phen$, $Ir(ppy)_3$, and BCzVBi, respectively, have been used as light-emitting dyes in organic light-emitting diodes with high color purity as well as high PLQY.[29–31] In fact, $Eu(TTA)_3Phen$, $Ir(ppy)_3$, and BCzVBi were selected because they absorb light in the UV range, but rarely absorb light in the visible range. Both the EVA and LDS dyes are soluble in organic solvents (e.g., chloroform, chlorobenzene, and tetrahydrofuran), which simplifies the LDS film fabrication process and supports the uniform dispersion of the dyes in the EVA film. The LDS films were fabricated by the simple drying of EVA solution with dye on a substrate (Figure S1). The thickness of the LDS film can be controlled by the EVA concentration, solution volume, and substrate area. A large free-standing LDS film can be easily obtained by detaching a thick LDS film from the fluorinated surface of a large Si substrate (Figure S2). The thickness of flat and textured LDS films was 206 and 240 μm, respectively (Figure S3). When the dye concentration was higher than the critical point, aggregation of the dyes was observed in EVA along with the increase in haze (Figure S4). The concentrations of $Eu(TTA)_3Phen$, $Ir(ppy)_3$, and BCzVBi in the EVA were optimized to 0.50, 0.05, and 0.10 wt%, respectively. Figure 1B shows the schematic illustration of the lossless color tuning of perovskite/Si tandem cells with LDS AR films with UV-selective absorption. When sunlight illuminates the perovskite/Si tandem cell with an LDS AR film with UV-selective absorption (Figure 1B), UV light, which is originally absorbed by the top transparent electrode and electron transport layer, can be absorbed by the LDS dyes. After the UV absorption, $Eu(TTA)_3Phen$, $Ir(ppy)_3$, and BCzVBi emit red, green, and blue light both inside and outside of the perovskite/Si tandem cells. The light emitted inside of the PV cells contributes to additional light absorption of the perovskite/Si tandem cells and the light emitted outside can be used to tune the color of the perovskite/Si tandem cells. Due to the UV absorbance of the LDS dyes and high transparency of EVA,[32,33] LDS AR film can maintain a high transparency in the visible and infrared ranges while effectively absorbing the UV light.

To confirm the UV-selective absorption and high color purity of $Eu(TTA)_3Phen$, $Ir(ppy)_3$, and BCzVBi in the EVA film, the photoluminescence (PL) and PL excitation (PLE) spectra of the LDS films were analyzed (Figure 2A). For the successful color tuning by LDS, sufficient light must be emitted from LDS dyes through the sufficient absorption of photons from sunlight as well as effective conversion with a high PLQY. The $Eu(TTA)_3Phen$, one of the lanthanide complexes, shows UV-selective absorption at wavelengths shorter than 400 nm and red emission with a sharp PL peak at 613 nm. The high absorption of UV and large Stokes shift of $Eu(TTA)_3Phen$ are possible because the antenna ligand TTA absorbs UV light up to 400 nm and the absorbed energy is transferred to the Eu ion.[34]

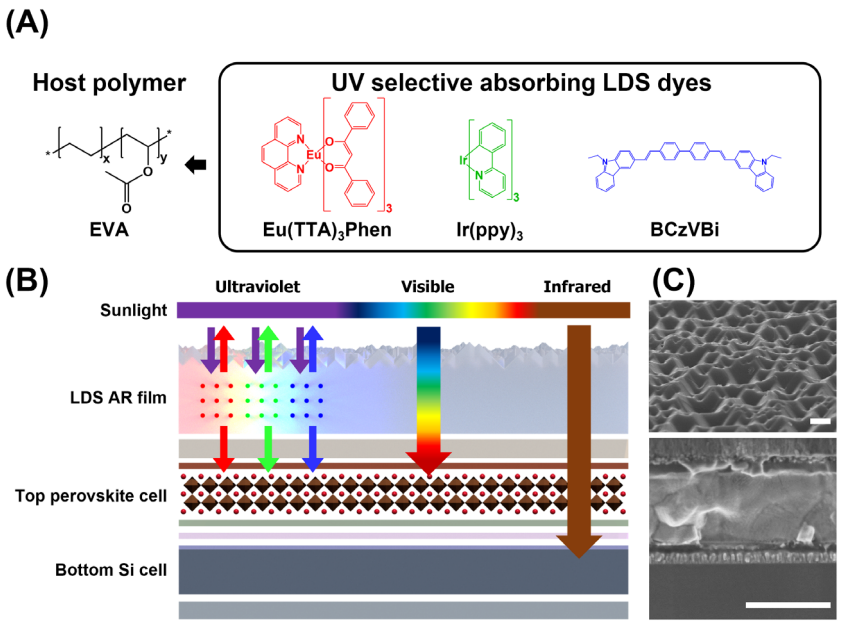

FIGURE 1 UV selective absorbing LDS AR film. (A) Chemical structures of EVA, $Eu(TTA)_3Phen$, $Ir(ppy)_3$, and BCzVBi. (B) Schematic illustration of the UV LDS AR film for perovskite/Si tandem cells. (C) 60°-tilted SEM image of textured EVA and cross-sectional SEM image of the perovskite/Si tandem cell (scale bar: 500 nm).

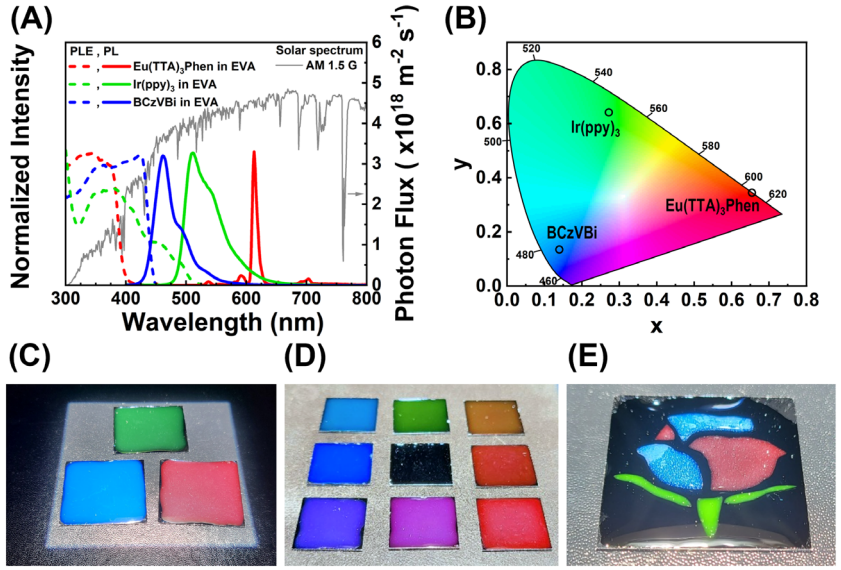

FIGURE 2 Optical properties of LDS dyes in EVA film. (A) Normalized PLE and PL spectra of $Eu(TTA)_3Phen$, $Ir(ppy)_3$, and BCzVBi in EVA films and photon flux of the AM 1.5 G solar spectrum. (B) Representation of the color coordinates of the PL spectra of $Eu(TTA)_3Phen$, $Ir(ppy)_3$, and BCzVBi in the CIE chromaticity diagram. (C) Photograph of the LDS films with red, green, and blue emissions of $Eu(TTA)_3Phen$, $Ir(ppy)_3$, and BCzVBi, respectively, under simulated solar light. (D) Photograph of LDS films with various color emissions obtained via the mixing of $Eu(TTA)_3Phen$, $Ir(ppy)_3$, and BCzVBi. (E) Photograph of the flower-shaped luminescence of various colored LDS films through the selective arrangement of LDS dyes.

After the nonradiative relaxation process in the Eu ion, effective red emission from the Eu ion ($^5D_0 \rightarrow {}^7F_2$ transition) occurs. The $Ir(ppy)_3$ was selected as a green LDS dye (PL peak at 514 nm) because it is a representative green-emitting dye with high color purity and high PLQY.[30] Although $Ir(ppy)_3$ has a wide absorption range and absorbs light from 400 to 500 nm, a small concentration of 0.05 wt% is sufficient for the color tuning with a small absorption in the visible range due to the high sensitivity of the human eye to green light (Figure S5). For blue-emitting LDS dye, even a small Stokes shift is enough to achieve UV-selective absorption, but the low sensitivity of human eyes to blue color (Figure S5) must be considered for color tuning and compensated by a higher light intensity. The BCzVBi, one of the organic dyes with high PLQY, was selected as blue LDS dye (PL peak at 461 nm). In addition to UV absorption, it shows high absorption up to 450 nm. Based on the additional absorption of BCzVBi between 400 and 450 nm, which shows a much higher photon flux than between 300 and 400 nm, BCzVBi can be used to effectively tune the color of PV cells to blue. The exact colors of light emitted from LDS dyes in EVA films can be represented by color coordinates (Figure 2B and Table 1). Based on the Commission Internationale de l'Eclairage (CIE) chromaticity diagram, the color coordinates of the PL spectra of $Eu(TTA)_3Phen$, $Ir(ppy)_3$, and BCzVBi in the EVA films confirm that the colors of light emitted from the dyes are red, green, and blue,

TABLE 1 The color coordinates of PL spectra of $Eu(TTA)_3Phen$, $Ir(ppy)_3$, and BCzVBi on the CIE 1931 chromaticity diagram.

	Color coordinates	
LDS dyes	***x***	***y***
$Eu(TTA)_3Phen$	0.654	0.345
$Ir(ppy)_3$	0.272	0.641
BCzVBi	0.140	0.135

respectively. The PLQYs of the LDS dyes in the EVA films are important for the effective color tuning and minimization of the PCE loss of the PV cell. The PLQYs of the LDS dyes in the EVA films were measured at the excitation wavelength of the highest absorption in the UV range. The PLQYs of $Eu(TTA)_3Phen$, $Ir(ppy)_3$, and BCzVBi, were calculated to be 70.11%, 68.68%, and 93.11%, respectively (Figure S6). Because all LDS dyes selectively absorb UV light, all LDS films that are formed on a Si substrate are almost colorless under indoor light without UV (Figure S7). Under simulated solar light including UV, the red, green, and blue emission was successfully observed in LDS films with $Eu(TTA)_3Phen$, $Ir(ppy)_3$, and BCzVBi, respectively (Figure 2C). While the full color tunability is an important aesthetic factor, color tuning based on structural color requires a non-intuitive and sophisticated structure to obtain the desired colors. However, because the three primary (red, green, and blue) colors of light emitted from LDS dyes can be separately emitted, full-color tuning based on the simple and intuitive mixing of the three LDS dyes is possible. The full-color tunability of LDS was confirmed by the simple mixing of $Eu(TTA)_3Phen$, $Ir(ppy)_3$, and BCzVBi. Orange, yellow, sky blue, indigo, and violet colors were successfully obtained in the LDS films (Figure 2D). Based on the simple color tuning via the luminescence of LDS dye, a free shape and flower-shaped luminescence with various colors can be achieved through the selective arrangement of LDS dyes (Figure 2E).

Because the LDS films are coated on front of the PV cell, the reflection at the surface is important for both the absorption of the LDS dye and PV cell. Fortunately, the host polymer EVA has a refractive index (~1.5) between that of low refractive air (refractive index of ~1.0) and that of the top transparent electrode of indium-doped zinc oxide (IZO, refractive index of ~2.0), which reduces the surface reflectance.[35,36] In addition to this favorable refractive index of the host polymer EVA, surface texturing was applied to EVA to effectively reduce the reflections over a wide wavelength range.[37,38] For the surface texturing of the EVA film, a Si substrate with random pyramid structure was used as a mold and the free-standing EVA film was laminated with thin spin-coated EVA film on the Si mold (Figure S1). The surfaces of flat EVA before surface texturing (Figure 3A) and textured EVA after surface texturing (Figure 3B) were analyzed by scanning electron microscopy (SEM). In contrast to the smooth, flat surface of flat EVA, textured EVA has an inverted pyramid-structured surface. Light reflected from the face of the inverted pyramid structure is directed back to the other face of the pyramid, effectively reducing the reflection of the incident light over a wide wavelength range. Furthermore, light transmitted through the textured surface is refracted, increasing the light path in the LDS film and PV cell.[39] The refractions of the light transmitted through flat EVA (Figure 3C) and textured EVA (Figure 3D) were optically compared with the changes of the background image and laser beam. With respect to flat EVA, the background image is clearly visible under both near and far conditions because the light is rarely refracted, whereas the background image is blurred under far conditions in textured EVA due to the refracted light. Due to the refraction along the square-directional planes of the inverted pyramid structure, the refraction of the light through the textured EVA could be clearly observed with the diamond-shaped patterned laser beam. To confirm the improvement of the transmittance by surface texturing and the compatibility of surface texturing and LDS, the transmittance spectra of flat EVA without dye, textured EVA without dye, and textured EVA with $Eu(TTA)_3Phen$, $Ir(ppy)_3$, and BCzVBi were measured with a UV–Vis–NIR spectrometer and integrating sphere. The total transmittance spectra are shown in Figure 3E. Textured EVA exhibits a higher transmittance than flat EVA, which is due to the reduced surface reflectance. After adding LDS dyes to textured EVA, all textured EVA films with LDS dyes have a lower transmittance in the UV range because of the absorption of the LDS dyes, but the transmittance of all textured EVA films remains unchanged outside the absorption range of the LDS dyes. This confirms that the anti-reflection properties of the textured EVA surface are compatible with color tuning with LDS. The diffuse transmittance (Figure S8) was also measured and haze spectra (Figure 3F) of each film were calculated based on the ratio of the diffuse to total transmittance. Because almost the area of the surface was tilted for the textured EVA as shown in Figure 3B, the haze of textured EVA is close to 100% in contrast to the negligible haze of flat EVA.[40] In the UV range in which LDS dyes are absorbed, the textured EVA with LDS dyes also shows a high haze concentration, which is due to the isotropic emission of LDS dyes.

After the successful fabrication of LDS AR films with dyes with UV-selective absorption, as described above,

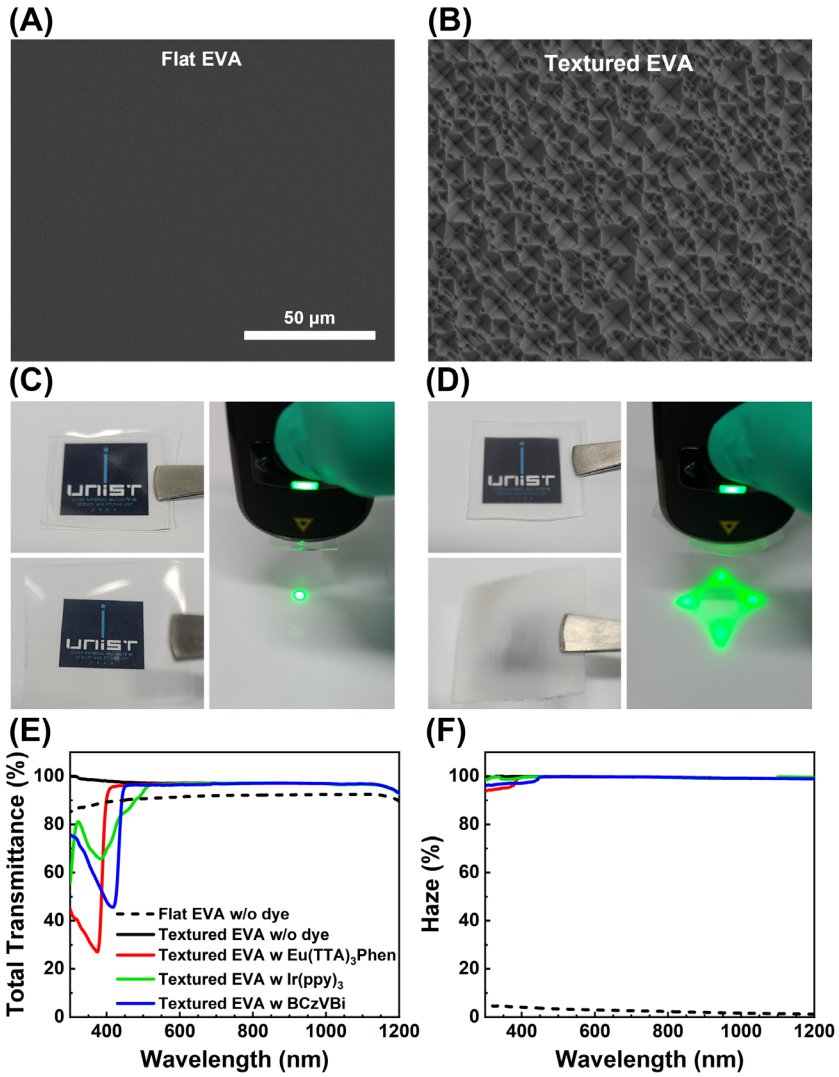

FIGURE 3 Surface texturing of EVA for LDS AR film. SEM top view images of (A) flat EVA and (B) textured EVA (scale bar: 50 μm). Photographs of the background image and laser beam through (C) flat EVA and (D) textured EVA. (E) Total transmittance spectra and (F) haze spectra of flat EVA without dye, textured EVA without dye, and textured EVA with $Eu(TTA)_3Phen$, $Ir(ppy)_3$, and BCzVBi.

the LDS AR films were applied to the perovskite/Si tandem cells to confirm the potential of color tuning as well as PCE increase (Figure 4A). The perovskite/Si tandem cells were fabricated with low-cost spin-on-dopant-based Al-BSF Si bottom cells and solution-processed perovskite top cells.[41] Although our tandem cell has an original color as well as high reflection due to the flat multilayered structure and different refractive indices, the LDS AR film on the front of the cell is expected to tune the color and reduce the reflection. The colors of the tandem cells with AR films depending on the LDS dyes are shown in Figure 4B. The original color of the tandem cell was purple (Figure S9). It changed to pink after attaching the thick surface-textured AR film without dye. Although our tandem cell with an AR film without dye has a pink color due to the remaining reflection, the colors of our tandem cells were successfully tuned to red, green, and blue using the LDS dyes $Eu(TTA)_3Phen$, $Ir(ppy)_3$, and BCzVBi, respectively. The light spectra of the perovskite/Si tandem cells with LDS AR films under AM 1.5 G simulated solar light were measured, and the colors were represented by color coordinates (Figure S10 and Table S1). To further enhance the vividness of the perovskite/Si tandem cells' color with LDS films, minimizing reflection in the visible range while maximizing the emission from the LDS dyes is necessary. In this regard, applying the LDS films on fully textured perovskite/Si tandem cells with negligibly low reflection[25] will significantly improve the vividness of color achieved with LDS films.

To confirm the PCE increase and lossless color-tuning of PV cell with LDS AR films, the current density–voltage (J–V) characteristics of the tandem cells with and without LDS AR films were measured (Figure 4C). The stabilized power output and hysteresis of perovskite tandem cells were also measured to confirm the PCEs (Figures S11 and S12). The J_{SC} and PCE of tandem cells significantly increased with the introduction of AR films and further increased due to the LDS dyes $Eu(TTA)_3Phen$ and BCzVBi. The LDS AR films attached on the outside of the

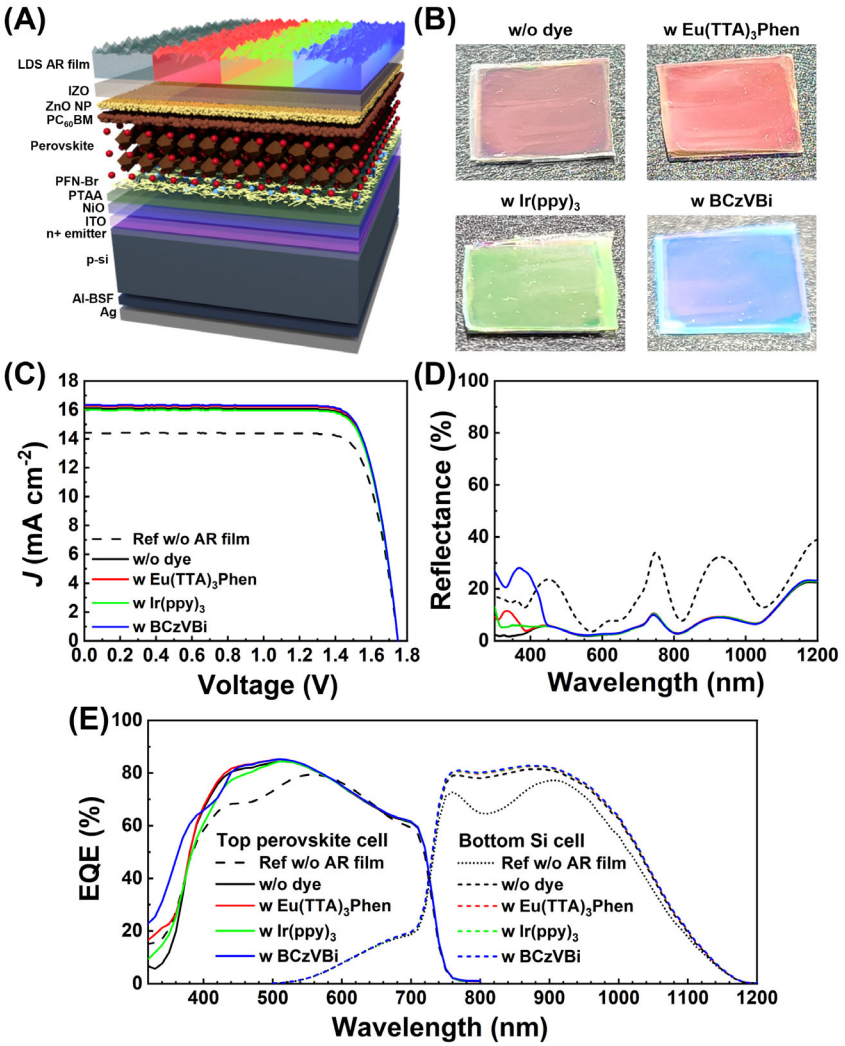

FIGURE 4 Perovskite/Si tandem cell with an LDS AR film. (A) Schematic diagram of the perovskite/Si tandem cell with an LDS AR film. (B) Photograph of the perovskite/Si tandem cells with AR films (without dye, with $Eu(TTA)_3Phen$, with $Ir(ppy)_3$, and with BCzVBi). (C) *J*–*V* curves, (D) reflectance spectra, and (E) EQE spectra of the perovskite/Si tandem cell without AR film and with AR film (without dye, with $Eu(TTA)_3Phen$, with $Ir(ppy)_3$, and with BCzVBi).

tandem cells did not affect the open-circuit voltage (V_{OC}) and fill factor (FF) of the tandem cells. To analyze the significant increase in the J_{SC}, the reflectance of tandem cells with LDS AR films was measured (Figure 4D). The tandem cell without AR film has a high reflectance with interference fringes in the NIR and visible ranges, whereas the tandem cells with AR films exhibit significantly reduced reflectance. The average reflectance in the NIR range (800–1200 nm) and visible range (400–800 nm) is 22.86% and 15.38% for the tandem cell without AR film, respectively, and decreases to 10.85% and 4.39%, respectively, for the tandem cells with AR films. The two reflectance peaks of the tandem cell in the visible range at ~450 and ~750 nm were consistent with the purplish-red color and the peak positions of the tandem cell with the 240 μm thick AR film did not shift. But the ratio between peak intensities at ~450 and ~750 nm was decreased with AR film, and the color of tandem cell was changed to pink. The reflectance spectra of tandem cells with AR films did not change due to the LDS dyes, except for an increase in the reflectance in the LDS dye absorption range based on the light emission from LDS dyes. These reduced reflectance spectra of tandem cells with LDS AR films are consistent with the increased transmittance spectra in Figure 3E, which is a result of the textured surface and good dispersion of UV-selective absorbing LDS dyes. With respect to the J_{SC} of the tandem cell, the current matching between the top and bottom cells is important to achieve the maximum J_{SC} and PCE. Therefore, the EQE spectra of the top perovskite cells and bottom Si cells were further analyzed to study the current matching and confirm the improved J_{SC} and PCE of tandem cells with LDS AR films (Figure 4E). Regarding the effectively reduced reflection over a wide wavelength range using surface-textured AR film, the perovskite/Si tandem cell with AR film exhibits a higher increase in the J_{SC} values calculated from the EQE spectra ($J_{SC.Calc}$) in the bottom Si cell (+1.53 mA cm^{-2}) than in the top perovskite cell (+1.01 mA cm^{-2}). By considering the different $J_{SC.Calc}$ increases of the top and bottom

TABLE 2 Summary of photovoltaic parameters[a] and $J_{SC.Calc}$ from the EQE spectra of perovskite/Si tandem cell without LDS AR film and with LDS AR film.

					$J_{SC.Calc}$ (mA cm^{-2})	
LDS AR film	**J_{SC} (mA cm^{-2})**	**V_{OC} (V)**	**FF (%)**	**PCE (%)**	**Top perovskite cell**	**Bottom Si cell**
Ref w/o AR film	14.42	1.75	80.22	20.24	15.27	14.78
w/o dye	16.12	1.75	80.17	22.62	16.28	16.31
w $Eu(TTA)_3Phen$	16.29	1.75	80.28	22.89	16.45	16.55
w $Ir(ppy)_3$	16.02	1.75	80.31	22.51	16.18	16.58
w BCzVBi	16.36	1.75	80.33	23.00	16.53	16.63

[a]Measured in a backward scan with a scan rate of 100 mV s^{-1}.

cells after applying AR film, current matching between the top perovskite and bottom Si cells was conducted by optimizing the bandgap and thickness of the perovskite layer (Table 2). The AR film-enhanced EQE is due to the reduced reflectance and does not depend on the LDS dye, except for the absorption range of LDS dye. The LDS dye on the front of the perovskite/Si tandem cells can absorb this UV light and convert it to the visible light which is mostly transmitted into the perovskite layer. Tandem cells with LDS dyes have improved EQE and $J_{SC.Calc}$ values in the UV range (+0.06, +0.01, and +0.21 mA cm^{-2} for $Eu(TTA)_3Phen$, $Ir(ppy)_3$, and BCzVBi, respectively) compared to that of tandem cells without LDS. These increased $J_{SC.Calc}$ values in the UV range based on LDS compensate for the EQE loss due to the additional absorption of $Ir(ppy)_3$ and BCzVBi in the visible range. Therefore, the $J_{SC.Calc}$ of the top perovskite cells with LDS dyes only show negligible changes compared to those of cells without LDS dye (relative changes of +1.0% for $Eu(TTA)_3Phen$, −0.6% for $Ir(ppy)_3$, and +1.5% for BCzVBi, respectively). Note that the PCE of the tandem cell with AR film further improved due to the LDS dye with UV-selective absorption and high PLQY. This suggests that the PCE (and color tunability) of PV cells can be further increased by developing novel LDS dyes with an optimized absorption range and higher PLQY. Finally, the PCE of the tandem cell strongly increased from 20.24% without AR film to 22.62% with AR film (∼11.8% relative increase). The PCE values were further increased or maintained after color tuning to red (PCE of 22.89%), blue (PCE of 23.00%), and green (PCE of 22.51%) using the LDS dyes $Eu(TTA)_3Phen$, BCzVBi, and $Ir(ppy)_3$, respectively.

The UV stability of perovskite/Si tandem cells with and without LDS AR films was tested (Figure S13).[42] Because of the absence of an interface between TiO_2 and perovskite in our perovskite/Si tandem cells, the UV stability of the perovskite/Si tandem cells without LDS AR film is even high after an UV dosage of 15 kWh m^{-2}. In addition, a high UV stability was observed for tandem cells with LDS AR films after an UV dosage of 15 kWh m^{-2}, confirming that the LDS dyes and EVA film did not degrade. The light stability of perovskite/Si tandem cells with LDS AR films was tested under continuous AM 1.5 G illumination in ambient air without encapsulation (Figure S14). With the high UV stability of LDS film, all tandem cells maintained a PCE over 90% of initial PCE after 16 days, indicating high light stability.

3 | CONCLUSION

In conclusion, this work successfully demonstrates lossless color tuning based on the use of LDS AR films with UV-selective absorption. The $Eu(TTA)_3Phen$, $Ir(ppy)_3$, and BCzVBi were selected as LDS dyes for the three primary colors red, green, and blue, respectively. Based on the simple drying of the LDS dyes in dispersed EVA solution, optimized LDS films with UV-selective absorption, high PLQY, and high color purity can be fabricated from LDS dyes that are well-dispersed in thick EVA films. Furthermore, LDS films are highly aesthetic in that full-color tuning and a free shape can be obtained by simple mixing and the selective arrangement of LDS dyes. In addition to the aesthetic color tuning of LDS film, AR can be achieved without affecting the color tuning by AR surface texturing compatible with color tuning based on the light emission from LDS dye. The perovskite/Si tandem cell with textured AR film exhibits highly enhanced J_{SC} and PCE values (11.8% relative increase) without decreases in the V_{OC} and FF. The colors of the perovskite/Si tandem cells with LDS AR film were successfully tuned to red, green, and blue with the LDS dyes $Eu(TTA)_3Phen$, $Ir(ppy)_3$, and BCzVBi respectively, yielding enhanced PCEs (13.1%, 11.2%, and 13.6% relative increase for $Eu(TTA)_3Phen$, $Ir(ppy)_3$, and BCzVBi, respectively). In contrast to color tuning with

structural color, lossless color tuning based on LDS AR films with UV-selective absorption is very promising in that it is a universal method that can be applied to all types of PV cells, it is a low-cost process, and the PCE loss is negligible. Moreover, further studies focused on developing dyes with more optimal optical properties, higher stability, and lower cost will make LDS color tuning for aesthetic PV cells even more promising. Additionally, as demonstrated in this study, the use of textured AR films with LDS dyes can be applied to other types of PV cells, increasing efficiency through reduced light reflection and providing additional J_{SC} gains with LDS dyes. Thus, our work not only showcases the potential of lossless color tuning with LDS AR films but also highlights avenues for future research and application in the field of aesthetic PV cells, with improved optical properties, cost-effectiveness, and broader compatibility with different PV technologies.

4 | EXPERIMENTAL SECTION

4.1 | Materials

Monocrystalline Si wafers (1–5 Ω cm, p-type, CZ, 525 μm), Spin on dopant (Filmtronics SOD P507), 1H,1H,2H,2H-perfluorooctyltriethoxysilane (FOTS, 98% Sigma-Aldirch), EVA (vinyl acetate 40 wt%, Sigma-Aldirch) $Eu(TTA)_3Phen$ (98.0%, TCI), $Ir(ppy)_3$ (purified by sublimation, 95.0%, TCI), BCzVBi (99.5%, EMindex), PTAA (M514, Mn 9150 g/mol, PDI = 1.53, Ossila), poly (9,9-bis(3′-(N,N-dimethyl)-N-ethylammoinium-propyl-2,7-fluorene)-alt-2,7-(9,9-dioctylfluorene))dibromide (PFN-Br, Mw 30 000 g/mol, PDI = 2, Sigma-Aldrich), formamidinium iodide (FAI, Greatcellsolar), cesium iodide (CsI, 99.998%, Alfa Aesar), methylammonium bromide (MABr, Greatcellsolar), lead iodide (PbI2, 99.99% TCI), lead bromide (PbBr2, 99.999% Alfa Aesar), $PC_{60}BM$ (99%, OSM), ZnO nanoparticle dispersions (Avantama N-10), were used as-received without further purification.

4.2 | Luminescent down-shifting film fabrications

Polished crystalline Si wafer was etched in KOH/IPA solution to form random pyramid textured Si wafer. Polished flat Si wafer and random pyramid textured Si wafer were treated by FOTS at 180°C for 3 h with moisture. EVA (200 mg/mL) solely or with LDS dyes (1 mg/mL for $Eu(TTA)_3Phen$, 0.1 mg/mL for $Ir(ppy)_3$, and 0.2 mg/mL for BCzVBi) were dissolved in chlorobenzene. 1 mL of EVA solution was drop casted onto a 3 cm × 3 cm flat Si substrate and dried at room temperature for 1 day. The dried EVA film on the flat Si was then heated at 100°C for 30 min to remove any residual chlorobenzene. After cooling, the dried EVA film was peeled off the flat Si to obtain a free-standing flat EVA film. To fabricate inverted pyramid textured EVA film, EVA solution was spin-coated onto the random pyramid textured Si wafer at 500 rpm for 60 s. The EVA spin-coated random pyramid textured Si substrate was then heated at 100°C for 10 min. The free-standing flat EVA film was laminated onto the EVA spin-coated random pyramid textured Si substrate while undergoing heating at 100°C. After cooling, the dried EVA film on the random pyramid textured Si substrate was peeled off to obtain free-standing inverted pyramid textured EVA film. EVA film with LDS dyes were fabricated in the same way as that mentioned above with EVA with LDS dye solution.

4.3 | Perovskite/Si tandem solar cell fabrication and measurement

The perovskite/Si tandem solar cells were fabricated and measured as described in the literature.[23,43] UV stability and light stability were tested in N_2 condition at RT without encapsulation and in ambient air at RT/35 RH% without encapsulation, respectively. The devices were exposed to the UV light and AM 1.5 G illumination, respectively in open circuit condition. VL-6.LC (Vilber) 365 nm UV lamp was used for UV stability test and LSH-7320 (Newport) LED solar simulator was used for light stability of tandem solar cells. The UV light intensity was calibrated to 20 mW/cm^2 by TM-213 UV-AB meter (Tenmars).

4.4 | Characterization

The thicknesses were measured using a surface profiler (a-step 250, KLA TENCOR instruments). The PL and PLE spectra were measured using a fluorometer (Cary Eclipse, Varian). PLQYs were measured using a spectrofluorometer (FP-8500ST, Jasco International). The SEM images were obtained using Nova NanoSEM 230 (FEI) operated at 10 kV. The transmittance and reflectance spectra were measured using an UV–Vis–NIR spectrometer with a diffuse reflectance accessory (Cary 5000 with DRA, Agilent Technology). Light spectra of solar cell under AM 1.5 G simulated solar light were measured using a spectrometer (HR 2000+, Ocean Optics) and optical fiber.

AUTHOR CONTRIBUTIONS

E.D.J. conceived the main idea. E.D.J. and C.U.K. inspired the project and prepared manuscript. E.D.J, C.U.K, Y.W.N., S.K.S. and Y.I.N. carried out the experiment. K.J.C. and M.H.S. supervised the project. All authors discussed the results and contributed to the final manuscript.

ACKNOWLEDGMENTS

This work was supported by the Technology Development Program to Solve Climate Changes through the NRF funded by the Ministry of Science and ICT (2019M1A2A2072416), the NRF grants funded by the Korea government (MSIT) (2019K1A3A1A61091347, 2021M3H4A1A02051234), and Korea Institute of Energy Technology Evaluation and Planning (KETEP) grant funded by the Korea government (MOTIE) (20213091010010, Super Solar Cells – Development of double junction solar cells, breakthrough for the theoretical limit of silicon solar cell efficiency [>35%]).

CONFLICT OF INTEREST STATEMENT

The authors declare no conflict of interest.

ORCID

Eui Dae Jung https://orcid.org/0000-0003-4848-0931
Chan Ul Kim https://orcid.org/0000-0001-5771-0116
Young Wook Noh https://orcid.org/0009-0007-6343-362X
Kyoung Jin Choi https://orcid.org/0000-0003-2884-8006
Myoung Hoon Song https://orcid.org/0000-0002-8106-7332

REFERENCES

1. IEA. *World Energy Outlook 2021*. Accessed December, 2021. https://www.iea.org/reports/world-energy-outlook-2021
2. Yoo JW, Jang J, Kim U, et al. Efficient perovskite solar mini-modules fabricated via bar-coating using 2-methoxyethanol-based formamidinium lead tri-iodide precursor solution. *Joule*. 2021;5(9):2420-2436. doi:10.1016/j.joule.2021.08.005
3. Min H, Lee DY, Kim J, et al. Perovskite solar cells with atomically coherent interlayers on SnO_2 electrodes. *Nature*. 2021;598(7881):444-450. doi:10.1038/s41586-021-03964-8
4. VDMA. *International Technology Roadmap for Photovoltaic (ITRPV) Twelfth Edition*. Accessed December, 2021. https://itrpv.vdma.org/web/itrpv/download
5. Hou Y, Aydin E, De Bastiani M, et al. Efficient tandem solar cells with solution-processed perovskite on textured crystalline silicon. *Science*. 2020;367(6482):1135-1140. doi:10.1126/science.aaz3691
6. Al-Ashouri A, Köhnen E, Li B, et al. Monolithic perovskite/silicon tandem solar cell with >29% efficiency by enhanced hole extraction. *Science*. 2020;370(6522):1300-1309. doi:10.1126/science.abd4016
7. Shen H, Walter D, Wu Y, et al. Monolithic perovskite/Si tandem solar cells: pathways to over 30% efficiency. *Adv Energy Mater*. 2020;10(13):1902840. doi:10.1002/aenm.201902840
8. Wang H, Li J, Dewi HA, Mathews N, Mhaisalkar S, Bruno A. Colorful perovskite solar cells: progress, strategies, and potentials. *J Phys Chem Lett*. 2021;12(4):1321-1329. doi:10.1021/acs.jpclett.0c03445
9. Yamaguchi M, Ozaki R, Nakamura K, et al. Development of high-efficiency solar cell modules for photovoltaic-powered vehicles. *Solar RRL*. 2022;6(5):2100429. doi:10.1002/solr.202100429
10. Chang NL, Zheng J, Wu Y, et al. A bottom-up cost analysis of silicon–perovskite tandem photovoltaics. *Prog Photovolt: Res Appl*. 2021;29(3):401-413. doi:10.1002/pip.3354
11. Lee K-T, Jang J-Y, Zhang J, Yang S-M, Park S, Park HJ. Highly efficient colored perovskite solar cells integrated with ultrathin subwavelength plasmonic nanoresonators. *Sci Rep*. 2017;7(1):10640. doi:10.1038/s41598-017-10937-3
12. Zhang W, Anaya M, Lozano G, et al. Highly efficient perovskite solar cells with tunable structural color. *Nano Lett*. 2015;15(3):1698-1702. doi:10.1021/nl504349z
13. Wang W, He Y, Qi L. High-efficiency colorful perovskite solar cells using TiO_2 nanobowl arrays as a structured electron transport layer. *Sci China Mater*. 2020;63(1):35-46. doi:10.1007/s40843-019-9452-1
14. Lee K-T, Fukuda M, Joglekar S, Guo LJ. Colored, see-through perovskite solar cells employing an optical cavity. *J Mater Chem C*. 2015;3(21):5377-5382. doi:10.1039/C5TC00622H
15. Lu J-H, Yu Y-L, Chuang S-R, Yeh C-H, Chen C-P. High-performance, semitransparent, easily tunable vivid colorful perovskite photovoltaics featuring Ag/ITO/Ag microcavity structures. *J Phys Chem C*. 2016;120(8):4233-4239. doi:10.1021/acs.jpcc.5b11144
16. Ramírez Quiroz CO, Bronnbauer C, Levchuk I, Hou Y, Brabec CJ, Forberich K. Coloring semitransparent perovskite solar cells via dielectric mirrors. *ACS Nano*. 2016;10(5):5104-5112. doi:10.1021/acsnano.6b00225
17. Lee K-T, Jang J-Y, Park SJ, Ok SA, Park HJ. Incident-angle-controlled semitransparent colored perovskite solar cells with improved efficiency exploiting a multilayer dielectric mirror. *Nanoscale*. 2017;9(37):13983-13989. doi:10.1039/C7NR04069E
18. Lee K-T, Jang J-Y, Ha NY, Lee S, Park HJ. High-performance colorful semitransparent perovskite solar cells with phase-compensated microcavities. *Nano Res*. 2018;11(5):2553-2561. doi:10.1007/s12274-017-1880-0
19. Yoo GY, Azmi R, Kim C, et al. Stable and colorful perovskite solar cells using a nonperiodic SiO_2/TiO_2 multi-nanolayer filter. *ACS Nano*. 2019;13(9):10129-10139. doi:10.1021/acsnano.9b03098
20. Day J, Senthilarasu S, Mallick TK. Improving spectral modification for applications in solar cells: a review. *Renew Energy*. 2019;132:186-205. doi:10.1016/j.renene.2018.07.101
21. Schlisske S, Mathies F, Busko D, et al. Design and color flexibility for inkjet-printed perovskite photovoltaics. *ACS Appl Energy Mater*. 2019;2(1):764-769. doi:10.1021/acsaem.8b01829
22. Zheng J, Mehrvarz H, Liao C, et al. Large-area 23%-efficient monolithic perovskite/homojunction-silicon tandem solar cell with enhanced UV stability using down-shifting material. *ACS Energy Lett*. 2019;4(11):2623-2631. doi:10.1021/acsenergylett.9b01783

23. Lee S, Kim CU, Bae S, et al. Improving light absorption in a perovskite/Si tandem solar cell via light scattering and UV-down shifting by a mixture of SiO_2 nanoparticles and phosphors. *Adv Funct Mater*. 2022;32(35):2204328. doi:10.1002/adfm.202204328
24. Chen B, Yu Z, Liu K, et al. Grain engineering for perovskite/silicon monolithic tandem solar cells with efficiency of 25.4%. *Joule*. 2019;3(1):177-190. doi:10.1016/j.joule.2018.10.003
25. Sahli F, Werner J, Kamino BA, et al. Fully textured monolithic perovskite/silicon tandem solar cells with 25.2% power conversion efficiency. *Nat Mater*. 2018;17(9):820-826. doi:10.1038/s41563-018-0115-4
26. Uekert T, Solodovnyk A, Ponomarenko S, et al. Nanostructured organosilicon luminophores in highly efficient luminescent down-shifting layers for thin film photovoltaics. *Sol Energy Mater Sol Cells*. 2016;155:1-8. doi:10.1016/j.solmat.2016.04.019
27. Klampaftis E, Richards BS. Improvement in multi-crystalline silicon solar cell efficiency via addition of luminescent material to EVA encapsulation layer. *Prog Photovolt: Res Appl*. 2011;19(3):345-351. doi:10.1002/pip.1019
28. Gavriluta A, Fix T, Nonat A, Slaoui A, Guillemoles J-F, Charbonnière LJ. Tuning the chemical properties of europium complexes as downshifting agents for copper indium gallium selenide solar cells. *J Mater Chem A*. 2017;5(27):14031-14040. doi:10.1039/C7TA02892J
29. Freund C, Porzio W, Giovanella U, et al. Thiophene based europium β-diketonate complexes: effect of the ligand structure on the emission quantum yield. *Inorg Chem*. 2011;50(12):5417-5429. doi:10.1021/ic1021164
30. Hofbeck T, Yersin H. The triplet state of fac-Ir(ppy)$_3$. *Inorg Chem*. 2010;49(20):9290-9299. doi:10.1021/ic100872w
31. Chou H-H, Chen Y-H, Hsu H-P, Chang W-H, Chen Y-H, Cheng C-H. Synthesis of diimidazolylstilbenes as n-type blue fluorophores: alternative dopant materials for highly efficient electroluminescent devices. *Adv Mater*. 2012;24(43):5867-5871. doi:10.1002/adma.201202222
32. Yuwawech K, Wootthikanokkhan J, Tanpichai S. Enhancement of thermal, mechanical and barrier properties of EVA solar cell encapsulating films by reinforcing with esterified cellulose nanofibres. *Polym Test*. 2015;48:12-22. doi:10.1016/j.polymertesting.2015.09.007
33. Sven L, Jan C, Guy D, et al. The use of the adding-doubling method for the optical optimization of planar luminescent down shifting layers for solar cells. *Opt Express*. 2014;22(S3):A765-A778. doi:10.1364/OE.22.00A765
34. Shahi PK, Singh AK, Singh SK, Rai SB, Ullrich B. Revelation of the technological versatility of the Eu(TTA)$_3$Phen complex by demonstrating energy harvesting, ultraviolet light detection, temperature sensing, and laser applications. *ACS Appl Mater Interfaces*. 2015;7(33):18231-18239. doi:10.1021/acsami.5b06350
35. Vogt MR, Holst H, Schulte-Huxel H, et al. Optical constants of UV transparent EVA and the impact on the PV module output power under realistic irradiation. *Energy Procedia*. 2016;92:523-530. doi:10.1016/j.egypro.2016.07.136
36. Kuo S-Y, Hsieh M-Y, Han H-V, et al. Flexible-textured polydimethylsiloxane antireflection structure for enhancing omnidirectional photovoltaic performance of Cu(In,Ga)Se_2 solar cells. *Opt Express*. 2014;22(3):2860-2867. doi:10.1364/OE.22.002860
37. Bush KA, Manzoor S, Frohna K, et al. Minimizing current and voltage losses to reach 25% efficient monolithic two-terminal perovskite–silicon tandem solar cells. *ACS Energy Lett*. 2018;3(9):2173-2180. doi:10.1021/acsenergylett.8b01201
38. Jošt M, Köhnen E, Morales-Vilches AB, et al. Textured interfaces in monolithic perovskite/silicon tandem solar cells: advanced light management for improved efficiency and energy yield. *Energ Environ Sci*. 2018;11(12):3511-3523. doi:10.1039/C8EE02469C
39. Ulbrich C, Gerber A, Hermans K, Lambertz A, Rau U. Analysis of short circuit current gains by an anti-reflective textured cover on silicon thin film solar cells. *Prog Photovolt: Res Appl*. 2013;21(8):1672-1681. doi:10.1002/pip.2249
40. Hwang I, Choi D, Lee S, et al. Enhancement of light absorption in photovoltaic devices using textured polydimethylsiloxane stickers. *ACS Appl Mater Interfaces*. 2017;9(25):21276-21282. doi:10.1021/acsami.7b04525
41. Kim CU, Yu JC, Jung ED, et al. Optimization of device design for low cost and high efficiency planar monolithic perovskite/silicon tandem solar cells. *Nano Energy*. 2019;60:213-221. doi:10.1016/j.nanoen.2019.03.056
42. Holzhey P, Saliba M. A full overview of international standards assessing the long-term stability of perovskite solar cells. *J Mater Chem A*. 2018;6(44):21794-21808. doi:10.1039/C8TA06950F
43. Bae S, Noh YW, Park D-S, Song MH, Choi S-W. Development of colored perovskite solar cells using cholesteric helicoidal superstructures. *Nano Energy*. 2022;93:106801. doi:10.1016/j.nanoen.2021.106801

SUPPORTING INFORMATION

Additional supporting information can be found online in the Supporting Information section at the end of this article.

How to cite this article: Jung ED, Kim CU, Noh YW, et al. Aesthetic and efficient perovskite/Si tandem solar cells using luminescent down-shifting textured anti-reflection films. *EcoMat*. 2023;5(10):e12399. doi:10.1002/eom2.12399